Original article

Biodistribution of [89]Zr-oxine-labeled human bone marrow-derived mesenchymal stem cells by micro-PET/computed tomography imaging in Sprague–Dawley rats

Shuzhe Wang[a,b,*], Yan Wang[b,*], Bohua Xu[c,*], Tian Qin[c], Yupeng Lv[c], Heng Yan[c], Yifei Shao[c], Yangyang Fang[c], Shaoqiu Zheng[c,d,e] and Yunliang Qiu[b]

Purpose To develop a method for labeling human bone marrow mesenchymal stem cells (hMSCs) with [89]Zr-oxine to characterize the biodistribution characteristics of hMSCs in normal Sprague–Dawley (SD) rats in real-time by micro-PET–computed tomography (micro-PET/CT) imaging.

Methods [89]Zr-oxine complex was synthesized from [89]Zr-oxalate and 8-hydroxyquinoline (oxine). After hMSCs were labeled with the [89]Zr-oxine complex, the radioactivity retention, viability, proliferation, apoptosis, differentiation, morphology, and phenotype of labeled cells were assessed. The biodistribution of [89]Zr-oxine-labeled hMSCs in SD rats was tracked in real-time by micro-PET/CT imaging.

Results The cell labeling efficiency was 52.6±0.01%, and [89]Zr-oxine was stably retained in cells (66.7±0.9% retention on 7 days after labeling). Compared with the unlabeled hMSCs, [89]Zr-oxine labeling did not affect the biological characteristics of cells. Following intravenous administration in SD rats, labeled hMSCs mainly accumulated in the liver (7.35±1.41% ID/g 10 days after labeling, $n = 6$) and spleen (8.48±1.20% ID/g 10 days after labeling, $n = 6$), whereas intravenously injected [89]Zr-oxalate mainly accumulated in the bone (4.47±0.35% ID/g 10 days after labeling, $n = 3$).

Conclusion [89]Zr-oxine labeling and micro-PET/CT imaging provide a useful and non-invasive method of assessing the biodistribution of cell therapy products in SD rats. The platform provides a foundation for us to further understand the mechanism of action and migration dynamics of cell therapy products. *Nucl Med Commun* 43: 834–846 Copyright © 2022 The Author(s). Published by Wolters Kluwer Health, Inc.

[a]College of Chemistry and Chemical Engineering, Shanghai University of Engineering Science, [b]Toxicology Department of China Academy of Pharmaceutical Industry Shanghai InnoStar Biotechnology Co. Ltd, Shanghai, [c]Radiographic Evaluation Department of InnoStar Biotechnology Nantong Co. Ltd, Nantong, [d]Jiangxi University of Traditional Chinese Medicine, Nanchang and [e]Yangtze Delta Advanced Research Institute, Yangtze Delta Pharmaceutical College Nantong, Jiangsu, China

Correspondence to Yunliang Qiu, MD, Shanghai InnoStar Biotechnology Co., Ltd, No. 199, Guoshoujing Road, Shanghai 201203, China
Tel/fax: +86 13816259345; e-mail: ylqiu@ncdser.cn

*Shuzhe Wang, Yan Wang and Bohua Xu are co-first authors.

Introduction

Cell therapy plays an important role in the treatment of a variety of diseases by repairing damaged tissue or replacing defective cells. The application of cell therapy requires a greater understanding of the fate of cells after transplantation. The technical guidelines for the study and evaluation of cell therapy products indicate that biodistribution and survival time after transplantation of cell therapy products are important factors affecting the effectiveness and safety of cell therapy products, and one or more appropriate cell tracing methods should be used to assess cell distribution, migration, and homing characteristics. The technical options for cell tracing include imaging, quantificational real-time PCR (Q-PCR), and immunohistochemistry. The latter two techniques require the sacrifice of animals after cell transplantation and the removal of corresponding tissues for testing, which has certain limitations. Molecular imaging technology can access the biodistribution and migration characteristics of transplanted cells in real-time after cell transplantation [1,2]. Many radionuclide cell labeling methods based on single-photon emission computed tomography (SPECT) [3–5] and PET [6–12] imaging have been used for cell tracking studies. Radionuclide labeled cells can detect picomolar concentrations or even lower concentrations of radiolabeled substances, therefore, radionuclide labeling is usually one of the methods of cell tracing. Compared to

PET, SPECT itself has lower sensitivity and resolution, so SPECT requires higher radioactivity, which can lead to cell damage. PET is at least 10 times more sensitive than SPECT, reducing the amount of radiation exposure of cells by a logarithm [13], and therefore, PET offers the potential to reduce cytotoxicity [14,15]. To achieve reduced radiation exposure while still achieving high sensitivity, high resolution, and sufficient duration to track cells for several days, a long-lived positron-emitting radioisotope is required. Zirconium 89 (^{89}Zr) has become an attractive radionuclide by monitoring labeled cells up to 2–3 weeks by PET imaging.

There are two commonly used methods for cell labeling with ^{89}Zr. One is to synthesize the ^{89}Zr-DBN complex by ^{89}Zr with p-NCS-Bz-DFO cheating, and the ^{89}Zr-DBN complex easily binds to cell membrane surface proteins to complete cell labeling. The other is the synthesis of the ^{89}Zr-oxine complex by ^{89}Zr-oxalate and 8-hydroxyquinoline (oxine), and the high lipid soluble oxine serves as the carrier of ^{89}Zr, making ^{89}Zr easy to penetrate cell membrane and firmly bind to the protein or cytoplasmic components within the cell. In this study, we used the second cell labeling method, which employed a two-step procedure (Fig. 1): (1) preparation of ^{89}Zr-oxine complex, (2) labeling of human bone marrow-derived mesenchymal stem cells (hMSCs) using ^{89}Zr-oxine complex. We assessed the radioactivity retention in cells after labeling as well as the viability, proliferation, apoptosis, differentiation, morphology, and phenotype post-labeling. In addition, the biodistribution and migration of ^{89}Zr-oxine-labeled hMSCs in normal Sprague–Dawley (SD) rats were traced by micro-PET–computed tomography (micro-PET/CT) imaging. The objective of this study was to establish a method for labeling hMSCs with ^{89}Zr-oxine complexes to characterize the biodistribution characteristics of hMSCs in normal SD rats in real-time by micro-PET/CT imaging.

Materials and methods
Rats and cells
All animal experiments were approved by the institutional animal care and use committee of our institution. SD rats were purchased from Zhejiang Weitonglihua Experimental Animal Technology Co., Ltd (Animal license No. SYXK Jiangsu 2021-0054). hMSCs were obtained from a commercial source (Cyagen, Suzhou, China) and cultured in hMSCs complete medium (hMSCs basal medium + 10% fetal bovine serum + 1% penicillin-streptomycin + 1% glutamine) after resuscitation. Cell cultures were maintained in a humidified atmosphere of 95% air with 5% carbon dioxide (CO_2) at 37 °C.

Synthesize of ^{89}Zr-oxine complex
^{89}Zr-oxine complex was generated by conjugating oxine to ^{89}Zr-oxalate at room temperature [6,8]. ^{89}Zr-oxalate (PerkinElmer, 150 μl, 160 MBq) was neutralized to pH 7.0–7.5 with 40 μl 1 M HEPES (Gibco) and 180 μl 1 M Na_2CO_3. Oxine in 1 M HEPES (500 μl, 1 mg/ml; Sigma-Aldrich, Saint Louis, USA) was added and spun in a vortex for 60 minutes at room temperature. Then, added 500 μl of chloroform, and extracted with shaking for 20 minutes, collected the lower layer (chloroform phase) liquid and dried it completely with a vacuum centrifuge concentrator. Finally, 100 μl of dimethyl sulfoxide (DMSO; Sigma-Aldrich) was added, sonicated to fully dissolved to obtain ^{89}Zr-oxine complex (100 μl, 95 MBq).

Cell labeling with ^{89}Zr-oxine complex
Cells were detached under mild conditions in 0.25% Trypsin-0.04% EDTA (Cyagen) for 3 minutes and centrifuged at 1200 rpm for 5 minutes. The cell pellet was resuspended in HHBS culture solution (Gibco, Hank's Balanced Salt Solution with 20 mM HEPES buffer) instead of complete medium, because resuspension of cells using complete medium would decrease labeling efficiency [8]. Diluted 50 μl of ^{89}Zr-oxine solution (40.0 MBq) to 5 ml (for adjusting DMSO ≤2%) with HHBS solution, then added to 4.5 ml hMSCs cell suspension (2.2×10^7 cells) and incubated for 30 minutes at room temperature for 30 minutes on a shaker (650 rpm). Then centrifuged at 1200 rpm for 5 minutes and determined the radioactivity in the supernatant and cell pellet with a radioactivity meter (CAPINTEC, CRC-55tR),

Fig. 1
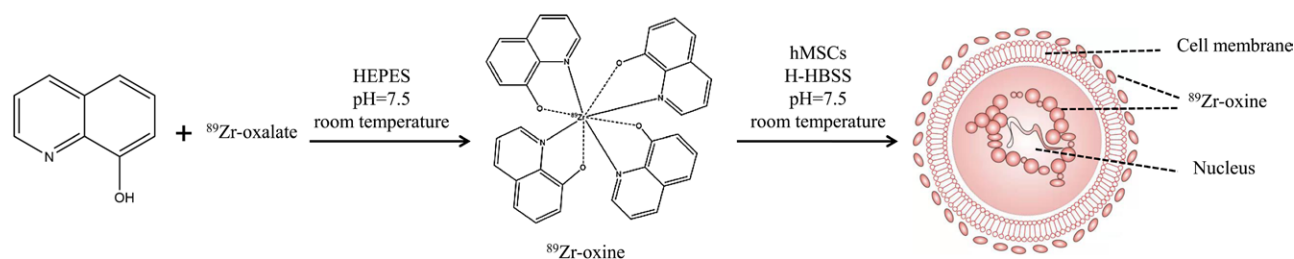
Schematic for the synthesis of ^{89}Zr-oxine and cell labeling.

respectively. Cells were then washed three times with 3 ml HHBS solution until the supernatant radioactivity/cell pellet radioactivity ≤10%. The cell labeling efficiency of ^{89}Zr-oxine was calculated by dividing the final cell pellet radioactivity by the total radioactivity used for labeling.

Determination of efflux of ^{89}Zr from ^{89}Zr-oxine-labeled cells

To assess retention of ^{89}Zr in cells, ^{89}Zr-oxine-labeled hMSCs were seeded into a 24-well culture plate at a density of 1×10^5 cells/well and cultured in an incubator at 37 °C, 95% air, and 5% CO_2. One (1), 2, 3, 4, 5, and 7 days after seeding, three wells were randomly selected each time point. The supernatant and cell pellet were collected separately, with a γ counter (Wizard2 3470) to detect the radioactivity count of each well supernatant and cell pellet separately. The percentage retention of ^{89}Zr in the labeled cells was calculated by cell pellet radioactivity count/(cell pellet radioactivity count + supernatant radioactivity count) × 100%.

Determination of cell viability and proliferation of ^{89}Zr-oxine-labeled cells

^{89}Zr-oxine-labeled and unlabeled hMSCs were each seeded in 24-well plates at a density of 1×10^5 cells/well. At 1, 2, 3, 4, 5, and 6 days after seeding, two wells were randomly selected from labeled and unlabeled cells each day, respectively, and cell viability was assessed by trypan blue (Solarbio) staining. Also, ^{89}Zr-oxine labeled and unlabeled hMSCs were inoculated into a 96-well plate at a density of 1×10^4 cells/well, respectively. One (1), 2, 3, 4, 5, and 7 days after inoculation, 10 µl of CCK-8 (Cell Counting Kit-8; Abcam, Cambridge, UK) reagent was added into three wells of labeled and 3 wells of unlabeled cells, and incubated in a CO_2 incubator for 2 h. The absorbance values of each well at 450 nm were then read using a microplate reader (SpectraMax i3x; Molecular Devices, Shanghai, China) to calculate the cell viability at each time point.

Determination of apoptosis of ^{89}Zr-oxine-labeled cells

Annexin V-FITC and propyl iodide (PI; Sigma-Aldrich) were used for fluorescent labeling of labeled and unlabeled hMSCs. Apoptosis was assessed by flow cytometry (CytoFLEX S; Beckman, Suzhou, China). Annexin V$^+$/PI$^-$ cells were considered to be early apoptotic cells and Annexin V$^+$/PI$^-$ cells were dead cells.

Determination of differentiation functionality of ^{89}Zr-oxine-labeled cells

To assess the effect of ^{89}Zr-oxine labeling on the ability of hMSCs to differentiate into osteoblast lineages, ^{89}Zr-oxine labeled and unlabeled hMSCs were inoculated into two six-well plates at a density of 2×10^5 cells/well respectively. Three wells selected in each plate

were incubated with hMSCs osteogenic differentiation medium (Cyagen) while the other three were incubated with hMSCs complete medium as un-induced control. The osteogenic differentiation medium consisted of FBS, penicillin-streptomycin, glutamine, ascorbate, β-Glycerophosphate, and dexamethasone. Osteogenic differentiation was determined using alizarin red staining.

The effect of ^{89}Zr-oxine labeling on the ability of hMSCs to differentiate into the adipogenic cell lineage was also tested using hMSCs adipogenic differentiation medium consisted of FBS, penicillin-streptomycin, glutamine, insulin, IBMX, rosiglitazone, and dexamethasone. Change the medium, which every 2–3 days, and after 3 weeks of incubation, the adipogenic differentiation effect of the cells was determined with oil-red O dye.

Analysis of Phenotype of ^{89}Zr-oxine-labeled cells

^{89}Zr-oxine-labeled and unlabeled hMSCs were evaluated for their surface expression of CD14, CD19, CD73, CD90, CD105, CD34, CD45, and HLA-DR with flow cytometry (CytoFLEX S; Beckman). Cells (10^6 cells in volume of 98 µl) were incubated with antibodies (2 µl) that had been labeled with different fluorescent dyes (CD73-PE-Vio770, 130-111-910; CD105-APC, 130-112-166; CD90-PE, 130-114-860; CD14-FITC, 130-110-518; CD19-FITC, 130-113-645; CD34-PE, 130-120-515; CD45-FITC, 130-110-631; HLA-DR-FITC, 130-111-788) for 30 minutes, and then washed cells twice with DPBS (washed off fluorescent antibodies that were not bound to cells). Added 500 µl of DPBS to resuspend the cell pellet, and the expression of surface markers for ^{89}Zr-oxine-labeled and unlabeled hMSCs was detected with flow cytometry. All antibodies were purchased from the Miltenyi Biotechnology Company.

Micro-PET/CT imaging of ^{89}Zr-oxine-labeled human bone marrow mesenchymal stem cells and ^{89}Zr-oxalate

A group of 3 male and 3 female rats were administered 3×10^6 ^{89}Zr-oxine-labeled hMSCs (approximately 3.7 MBq). An additional of 3 female rats were administered ^{89}Zr-oxalate (^{89}Zr-oxalate was first adjusted to neutrality with 1M Na_2CO_3 and then diluted with HHBS to the desired radioactivity) of the same radioactivity. Micro-PET/CT (Inveon, SIMENS, Berlin, Germany) scans of rats were performed sequentially at 1 h, 1 day, 3 days, 7 days, and 10 days after intravenous injection to obtain whole-body distribution images of radioactive signals at different time points. Before scanning, the rats were anesthetized with an isoflurane gas anesthesia machine (a mixture of 3% isoflurane and oxygen), and then the rats were held in a prone position and fixed in a micro-PET/CT scanner, and the rats were supplied with an anesthesia mask to inhale 1.5% isoflurane (a mixture of 1.5% isoflurane and oxygen) to maintain the rat's anesthesia state during imaging. The voltage of the CT scan was 80 kV. Inveon Acquisition Workplace software was used for image

acquisition and Inveon Research Workplace software was used for data processing. Image reconstruction used an ordered-subset expectation maximization algorithm. Image processing was performed by PMOD software and then the 3D regions of interest (ROIs) were manually plotted around the heart, liver, spleen, lungs, kidneys, brain, and bone tissue based on the contrast of CT soft tissues. The percentage of % injection dose per gram tissue (% ID/g) (see Tables S1 and S2, Supplemental digital content 1, *http://links.lww.com/NMC/A218*) and standardized uptake values (see Tables S3 and S4, Supplemental digital content 1, *http://links.lww.com/NMC/A218*) were calculated using the attenuation corrected ROIs value.

The management and use of animals during the experiments complied with the requirements in the guide of the care and use of laboratory animals issued by the US National Research Council, the administration of laboratory animals issued by the Chinese Science and Technology Commission in 1988, and the Jiangsu Provincial approach to the management of laboratory animals issued in 2008.

Statistical analysis
Statistical analysis and plotting were performed using SPSS 23.0 and GraphPad Prism 9 software. All data were expressed as mean ± SD. Statistical analysis was performed using Student's *t*-test and the one-way analysis of variance. A value of $P < 0.05$ or $P < 0.01$ was considered statistically significant difference.

Results
Labeling efficiency and cellular ^{89}Zr retention
2.2×10^7 hMSCs were incubated with 40.0 MBq ^{89}Zr-oxine for 30 minutes to obtain an average cell labeling efficiency of $52.6 \pm 0.01\%$ ($n = 2$), sufficient for imaging needs. Labeling efficiency of ^{89}Zr-oxine was higher than the previous methods [8], possibly due to the use of different cell types or higher cell concentrations in this study, resulting in the difference in the amount of intracellular proteins available for ^{89}Zr binding. The procedure resulted in an initial specific activity of approximately 1.3 MBq/10^6 cells. The percentage retention of ^{89}Zr-oxine in the cells on days 1, 2, 3, 4, 5, and 7 after labeling was $87.3 \pm 1.9\%$, $86.7 \pm 0.2\%$, $83.3 \pm 0.8\%$, $81.1 \pm 1.0\%$, $78.1 \pm 0.9\%$, and $66.7 \pm 0.9\%$, respectively (Fig. 2). The retention rate of ^{89}Zr-oxine in cells decreased in a time-dependent manner.

Cell viability, proliferation, and apoptosis of ^{89}Zr-oxine-labeled human bone marrow mesenchymal stem cells
To assess ^{89}Zr-oxine cytotoxicity, hMSCs were labeled with different radiation doses of ^{89}Zr-oxine (2.2, 3.7, and 5.6 MBq/10^6 cells). Labeling efficiency correlated negatively with ^{89}Zr-oxine amount, with the highest labeling efficiency (59.4%) and cell viability (84.9%) at the lowest doses of ^{89}Zr-oxine (see Table S5, Supplemental digital content 1, *http://links.lww.com/NMC/A218*). High

labeling efficiency and viability could still be achieved when the amounts of cells and ^{89}Zr-oxine were scaled up according to the ratio of 2.2 MBq/10^6 cells (see Table S6, Supplemental digital content 1, *http://links.lww.com/NMC/A218*), and this ratio of cells and ^{89}Zr-oxine was used for subsequent experiments. Within 6 days after labeling, ^{89}Zr-oxine-labeled hMSCs exhibited cell viability similar to unlabeled cells (Fig. 3, $P = 0.78$). The results of the CCK-8 assay showed that the proliferation level of ^{89}Zr-oxine-labeled hMSCs was slightly reduced compared to unlabeled cells 3 days after labeling (Fig. 4, $P < 0.01$). Apoptosis detection by flow cytometry showed that the apoptosis rate of ^{89}Zr-oxine-labeled hMSCs (12.0%) was slightly higher than that of unlabeled cells (6.4%) (Fig. 5).

^{89}Zr-oxine labeling did not affect the characterization of human bone marrow mesenchymal stem cells
Inverted phase-contrast microscopy showed that ^{89}Zr-oxine-labeled hMSCs had the same typical fibroblast-like morphology as unlabeled hMSCs. (see Fig. S1, Supplemental digital content 1, *http://links.lww.com/NMC/A218*). In addition, we found that ^{89}Zr-oxine-labeled hMSCs had the same differentiation function as unlabeled hMSCs. After 3 weeks of adipogenic differentiation induction, a large number of adipocytes were produced in both ^{89}Zr-oxine-labeled and unlabeled hMSCs, and lipid-filled vesicles were stained red with oil-red O (Fig. 6a and c). After 3 weeks of induction culture for osteogenesis differentiation, there were large amounts of calcium nodule deposition in both the ^{89}Zr-oxine labeled and unlabeled hMSCs, stained red by alizarin red (Fig. 6e and g), and the uninvited cultured cells acted as a negative control (Fig. 6b, d, f, and h).

The effect of ^{89}Zr-oxine labeling on hMSCs specific surface marker expression was evaluated by flow cytometry according to the ISCT-approved minimum criteria for identifying mesenchymal stromal cells (MSCs) [16]. ^{89}Zr-oxine-labeled hMSCs showed the same surface marker expression as unlabeled cells (positive expression of CD73, CD90, and CD105; negative expression of CD14, CD19, HLA-DR, CD34, and CD45) (Fig. 7).

In-vivo tracking of ^{89}Zr-oxine-labeled human bone marrow mesenchymal stem cells with micro-PET/CT
The biodistribution of radioactive signal was visualized and quantified by micro-PET/CT at 1 hour and 1, 3, 7, 10 days after injection of ^{89}Zr-oxine-labeled hMSCs and ^{89}Zr-oxalate (Fig. 8, Figs. S2 and S3, Supplemental digital content 1, *http://links.lww.com/NMC/A218*). Consistent with previous studies [8,12], the distribution of ^{89}Zr-oxine-labeled hMSCs was mainly concentrated in the lungs ($17.90 \pm 3.63\%$ ID/g) 1 hour after injection (Fig. 9) and migrated to the liver ($10.55 \pm 2.17\%$ ID/g) and spleen ($9.25 \pm 1.17\%$ ID/g) 1 day after injection (Fig. 10). From 1 h to 1 day after injection, pulmonary uptake decreased

Fig. 2
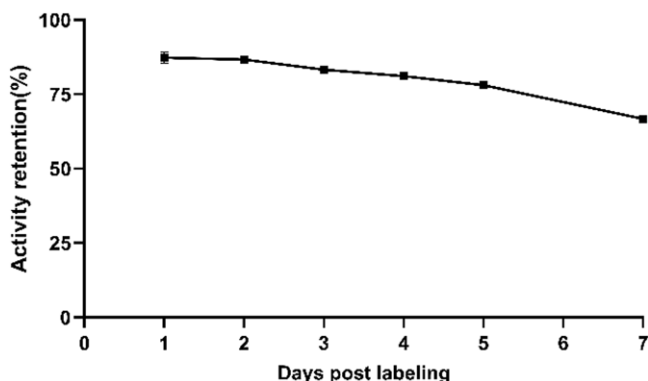
Retention of ^{89}Zr in hMSCs at 1, 2, 3, 4, 5, and 7 days after labeling. Each point was representative of the mean ± SD of three determinations.

Fig. 3
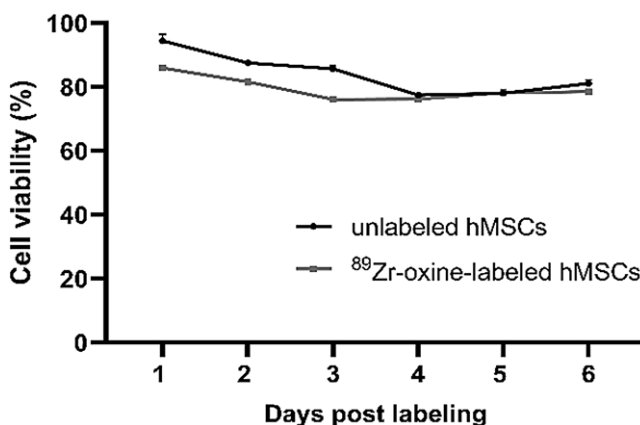
Determination of viability of ^{89}Zr-oxine-labeled hMSCs. ^{89}Zr-oxine-labeled cells demonstrated similar survival as compared with unlabeled cells up to 7 days after labeling ($P = 0.78$). Data were representative of two independent experiments. All data were expressed as the mean ± SD.

from $17.90 \pm 3.63\%$ ID/g to $0.66 \pm 0.18\%$ ID/g. Up to 10 days after injection, there was still a large intake in the liver ($7.35 \pm 1.41\%$ ID/g) and spleen ($8.48 \pm 1.20\%$ ID/g) (Fig. 11). Unlike the biodistribution of hMSCs, the biodistribution of ^{89}Zr-oxalate was relatively dispersed 1 h after injection, with a relatively high uptake in the heart ($3.77 \pm 0.75\%$ ID/g). Migration to bone ($3.57 \pm 0.06\%$ ID/g) was mainly seen 1 day after injection, and large uptakes ($4.77 \pm 0.35\%$ ID/g) were still visible in bone 10 days after injection. The biodistribution of ^{89}Zr-oxalate indicated that the low radioactivity seen in the bone ($0.96 \pm 0.33\%$ ID/g, 10 days after labeling) of rats injected ^{89}Zr-oxine-labeled hMSCs might be derived from free ^{89}Zr released from dead hMSCs.

Discussion

As we know, MSCs, whether from humans or from other species, have a low immunogenic cellular phenotype [17–19]. MSCs therapy is considered an effective immunomodulatory and regenerative therapy in a variety of animal models, including transplant models [20], experimental colitis [21], rheumatoid arthritis [22], bone/cartilage injury [23,24], and a number of other models. Although previous studies have described a series of immune responses related to the immunomodulatory effects of MSCs, such as inducing the production of cells with regulatory phenotypes, inhibiting inflammatory cells and secreting anti-inflammatory molecules [25–28], the mechanism of action of MSCs has not been fully determined, and the fate of cells after transplantation has not been fully understood [29]. Therefore, cell tracking technique is needed to assess cell biodistribution, which is helpful to further understand the mechanism of many emerging cell-based therapies. One of the most promising ways to monitor the biological distribution

Fig. 4
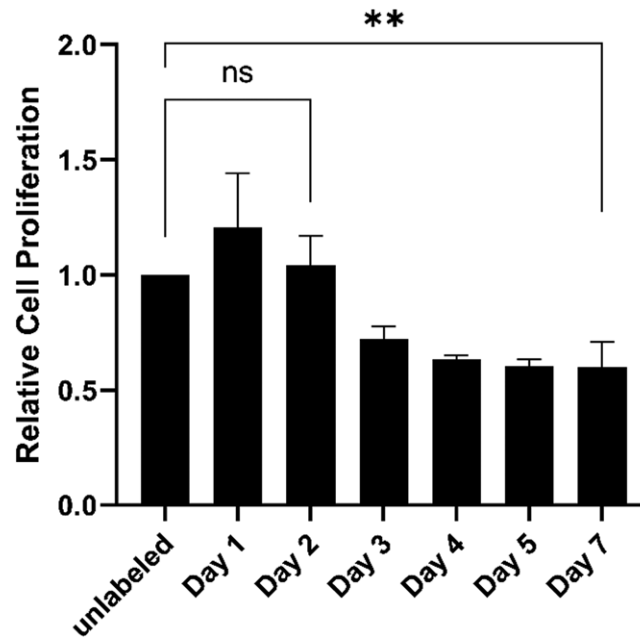
Determination of cell proliferation of [89]Zr-oxine-labeled hMSCs. The proliferative level of the [89]Zr-oxine-labeled hMSCs was significantly reduced from 3 to 7 days after labeling, as compared with that of unlabeled. Data were representative of three independent experiments. All data were expressed as the mean ± SD. **The difference was significant at the 0.01 level.

Fig. 5
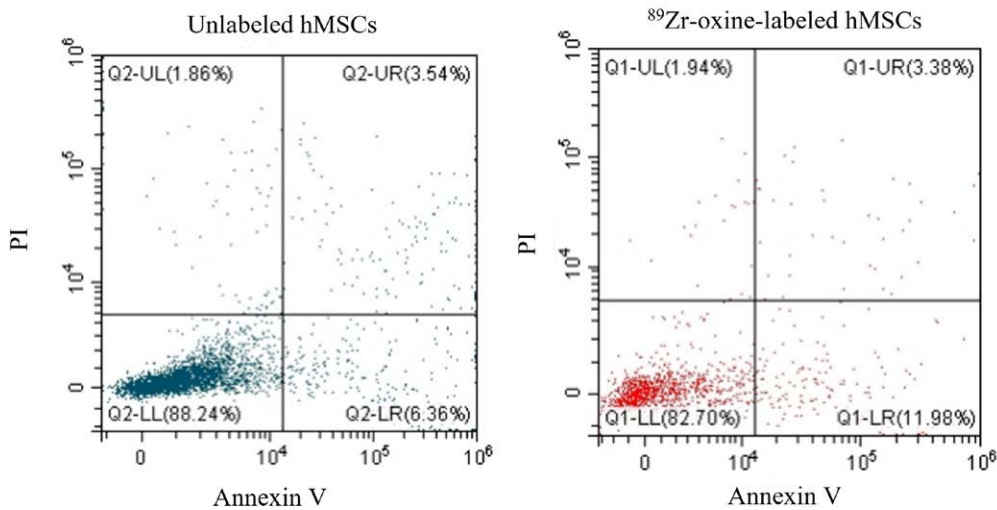
Determination of apoptosis of [89]Zr-oxine-labeled cells. Apoptosis of [89]Zr-oxine-labeled and unlabeled hMSCs was detected by flow cytometry, which showed that radioisotope labeling slightly increased the degree of apoptosis. $P > 0.05$, there was no statistically significant difference.

of MSCs is cell labeling with tracers such as [89]Zr-oxine. The effects of the [89]Zr-oxine marker on cell viability and proliferation have been reported [6,8,10–12], and these effects may vary depending on cell types. In this study, we evaluated the effects of the [89]Zr-oxine labeling on the cellular functionality and biological characteristics of hMSCs, analyzed the radioactivity retention, cell viability, proliferation, apoptosis, differentiation, morphology,

Fig. 6
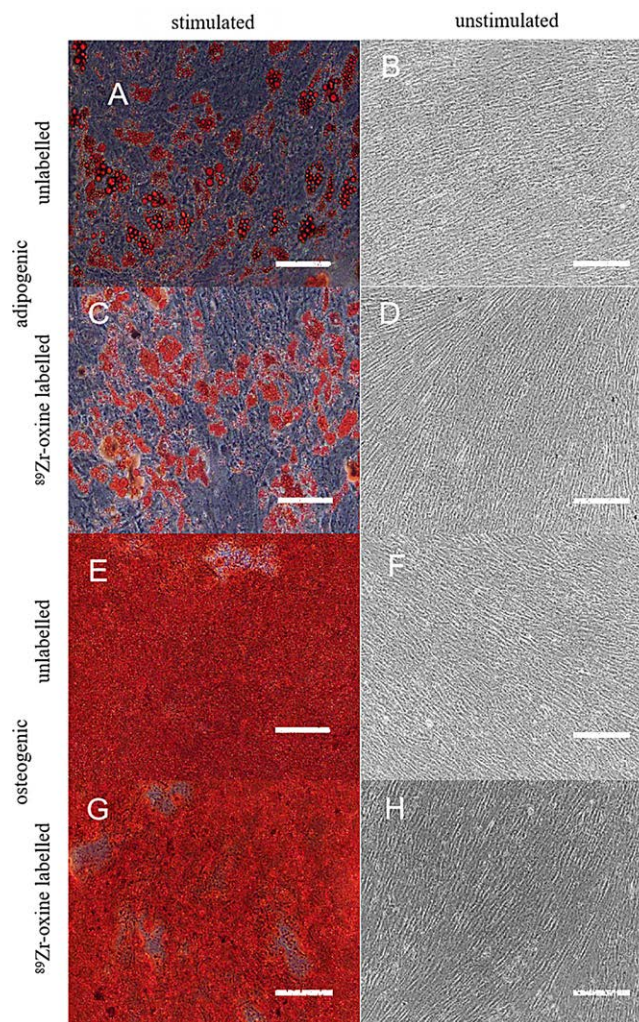
Determination of differentiation functionality of ^{89}Zr-oxine-labeled hMSCs. ^{89}Zr-oxine-labeled hMSCs were differentiated towards both the osteogenic (c) and the adipogenic (g) lineages as did as unlabeled cells (a, e), with uninduced cells (b, d, f, h) serving as negative controls. Bar = 100 μm.

and phenotype in cells after the ^{89}Zr-oxine labeling *in vitro*, and used micro-PET/CT to initially characterize the biodistribution and migration of cells in rats.

The trypan blue staining test showed that ^{89}Zr-oxine was incubated with hMSCs for 30 min at a labeled dose of 2.2 MBq/10^6 cells, with no negative effect on the viability of hMSCs. However, cell viability decreased significantly at labeled doses of 3.7 and 5.6 MBq/10^6 cells, suggesting that cell viability decreased in a dose-dependent manner after ^{89}Zr-oxine in-vitro labeling. The effect of the different radiation doses of ^{89}Zr-oxine on radioactivity retention in cells was also examined (Table S7, Supplemental digital content 1, *http://links.lww.com/ NMC/A218*), and as the same effect on cell viability, ^{89}Zr-oxine had a significant dose-dependent effect on

radioactivity retention in cells. The retention of ^{89}Zr in cells was the key to evaluate the success of labeling. Once ^{89}Zr-oxine enters the cell, the ^{89}Zr remains stably inside the living cell, and once the labeled cell dies, it causes the free ^{89}Zr to be released rapidly from the cell [8]. Therefore, cell mortality can be reflected according to the outflow rate of ^{89}Zr. We also tried labeling cells with a lower radioactive dose of ^{89}Zr-oxine (1.5 MBq/10^6 cells), but the specific radioactivity of the cells after labeling was too low to complete a continuous 10-day in-vivo tracer. Therefore, the labeling dose of 2.2 MBq/10^6 cells was used for subsequent study. Labeling efficiency of 52.6 ± 0.01% was achieved, which was sufficient for imaging needs. The retention of ^{89}Zr in cells decreased time-dependently, with intracellular retention of 66.7 ± 0.9% at 7 days after labeling

Fig. 7
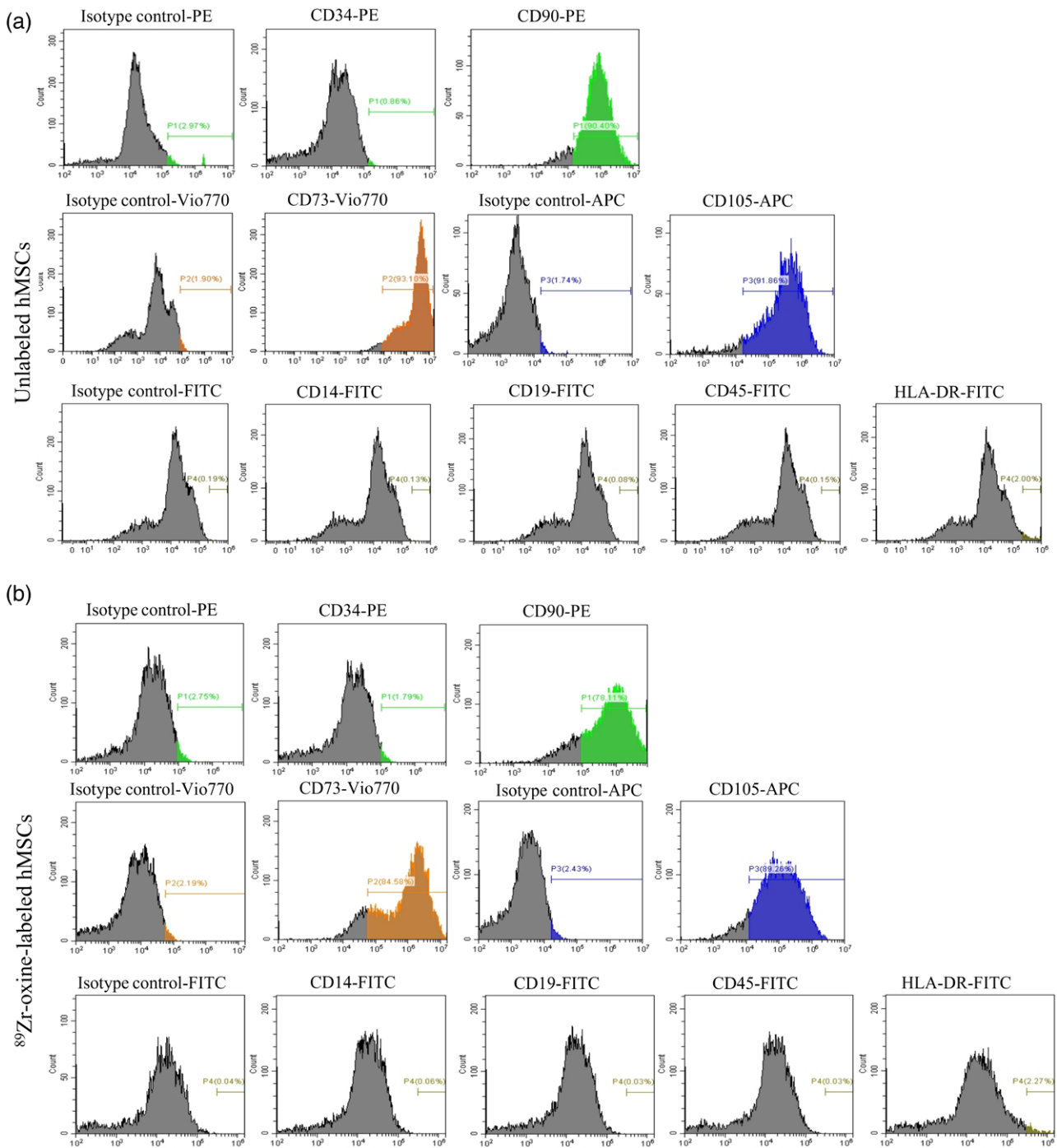
89Zr-oxine-labeled hMSCs showed surface marker expression same as that of unlabeled cells (positive expression of CD73, CD90, and CD105; negative expression of CD14, CD19, HLA-DR, CD34, and CD45).

(Fig. 2), compared with a recent study using ^{89}Zr-oxine labeling MSCTRAIL, and the retention of ^{89}Zr in cells was greatly improved in this study [12]. Within 6 days after labeling, ^{89}Zr-oxine-labeled hMSCs showed simar

viability to unlabeled cells (Fig. 3, $P = 0.78$). Compared to unlabeled cells, the ^{89}Zr-oxine labeling had a slight effect on cell proliferation, and cell proliferative activity decreased from 3 days after labeling (Fig. 4). Cells are

Fig. 8
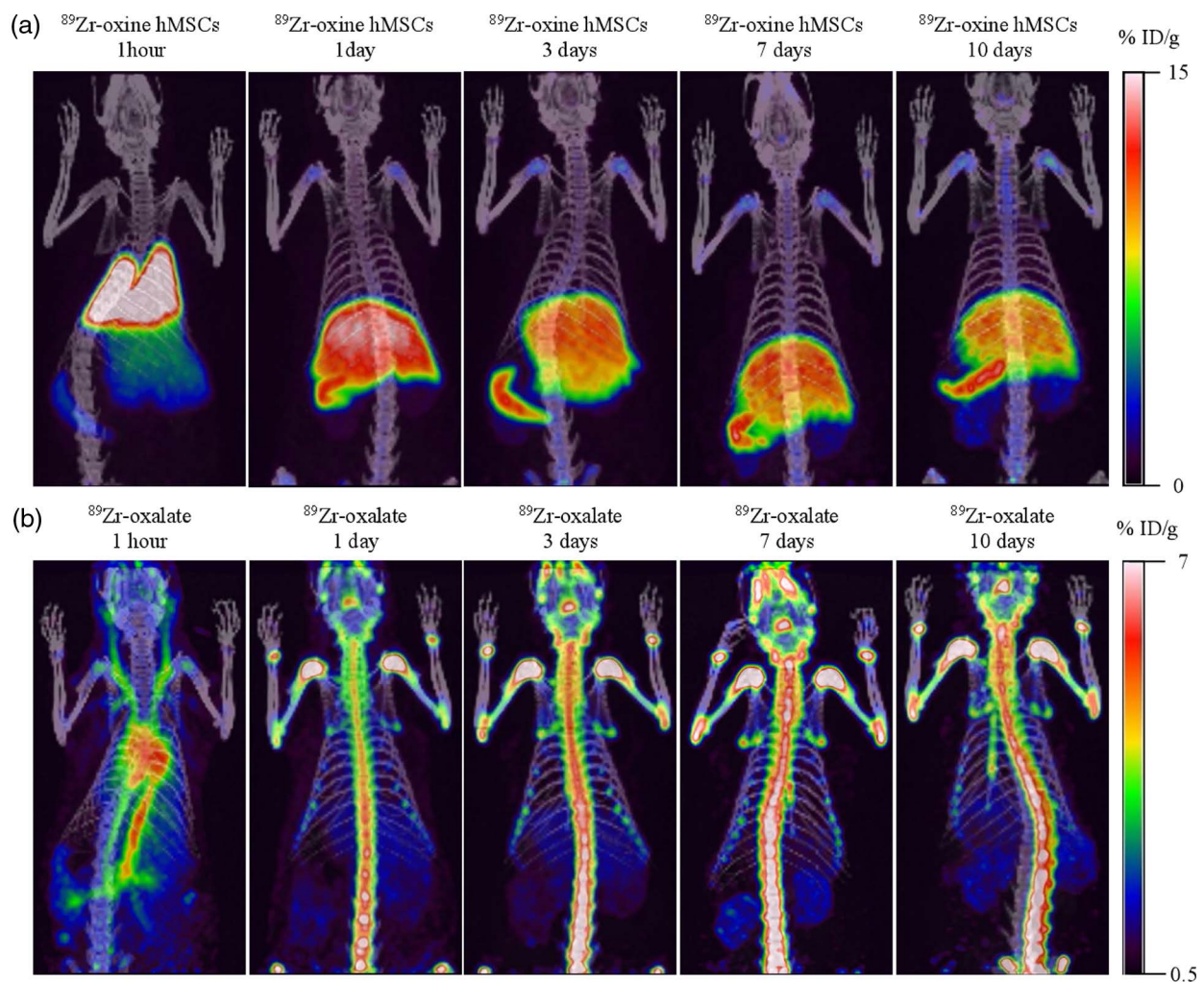
Micro-PET/CT images of ^{89}Zr-oxine-labeled hMSCs and ^{89}Zr-oxalate in SD rats. (a) PET/CT whole-body images of the biodistribution of ^{89}Zr-oxine-labeled hMSCs in SD rats over the following ten days ($n = 6$). (b) PET/CT whole-body images of the biodistribution of ^{89}Zr-oxalate in SD rats over the following ten days ($n = 3$).

known to be most sensitive to radioactivity during the division phase and lowest in the DNA synthesis phase, so it can be assumed that cells are in the DNA synthesis phase 1–2 days after seeding, and begin to enter the cell division phase 3 days after seeding. At this time, the sensitivity of cells to radioactivity is the highest, resulting in a large number of cells being killed, and a decrease in cell proliferation. ^{89}Zr-oxine labeling slightly increased the level of apoptosis (Fig. 5, $P > 0.05$), which may be related to repeated cleaning and blowing of cells during the cell labeling process, or may be related to radiotoxicity or chemical toxicity of oxine, but the overall effect was small. We also found that the ^{89}Zr-oxine labeling did not affect the basic stem cell properties [30]. ^{89}Zr-oxine-labeled hMSCs showed the persistence capability to differentiate into the adipogenic and osteogenic lineages (Fig. 6). In addition, ^{89}Zr-oxine labeling did not affect either the normal cell morphology of hMSCs or the expression of stem cell-specific surface markers (positive expression of CD73, CD90, and CD105; negative expression of CD14, CD19, HLA-DR, CD34, and CD45). If ^{89}Zr-oxine labeling interferes with cell function, it may result in differences in the actual distribution of labeled cells versus unlabeled cells. In conclusion, the labeling method used in this study did not interfere with the functional and biological characteristics of hMSCs.

We also observed the biodistribution and migration dynamics of intravenous ^{89}Zr-oxine-labeled hMSCs in normal SD rats with micro-PET/CT imaging. As expected, the overall biodistribution observed with ^{89}Zr-oxine-labeled

Fig. 9
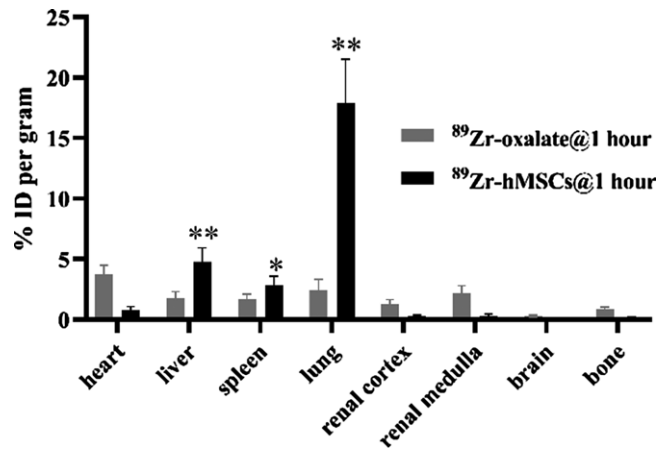
The biodistribution of ^{89}Zr-oxine-labeled hMSCs and ^{89}Zr-oxalate at 1 hour post-injection. ^{89}Zr-oxine-labeled hMSCs were mainly distributed in the lung (17.90±3.63% ID/g). The distribution of ^{89}Zr-oxalate was relatively discrete at 1 hour after injection, with signal uptake in the heart, liver, spleen, lung, kidney, and bone, and relatively higher uptake in the heart (3.77±0.75% ID/g). *: the difference from that of the control was significant at the $P < 0.05$ level. **: the difference from that of the control was significant at the $P < 0.01$ level. All data were expressed as means ± SD.
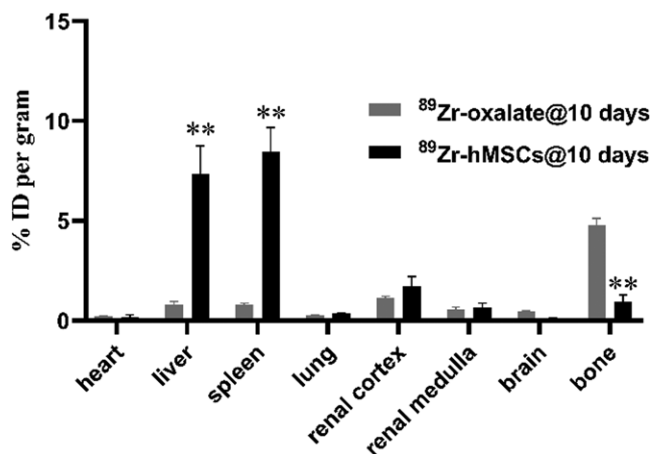
Fig. 10
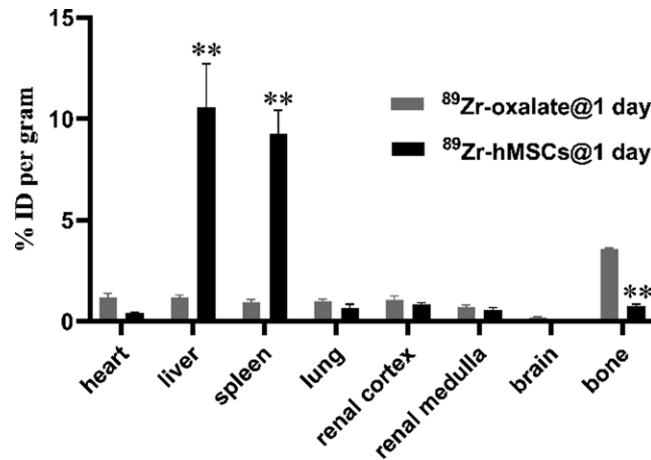
The biodistribution of ^{89}Zr-oxine-labeled hMSCs and ^{89}Zr-oxalate at 1 day post-injection. ^{89}Zr-oxine-labeled hMSCs were mainly distributed in the liver (10.55±2.17% ID/g) and spleen (9.25±1.17% ID/g). ^{89}Zr-oxalate was mainly distributed in the bone (3.57±0.06% ID/g). **The difference was significant from that of the control at $P < 0.01$ level. All data were expressed as means ± SD.

hMSCs (Fig. 8a, initially uptake in the lungs followed by migration to the liver, spleen, and bone) was consistent with earlier reports in mice imaging studies [12,31,32], as well as in clinical trials [33]. One hour after injection, most (66%) radioactive signals were found in the lungs, and small amounts were also found in the liver (18%) and spleen (10%). After 1 day, the level of radioactivity in the lungs (3%) decreased significantly, while the level of radioactivity in the liver (46%) and spleen (40%) increased significantly. Ten days after the injection, there was still a large amount of radioactivity in the liver (37%) and spleen (43%), in addition, a small amount of radioactivity (5%) was also found in the bone. Radioactivity in other organs was around background levels. As a control, we found that intravenously injected free ^{89}Zr-oxalate resulted in a relatively discrete distribution of ^{89}Zr-oxalate at 1 hour, with radioactivity uptake in heart, liver, spleen, lung, kidney, and bone tissue but relatively high uptake in heart (3.77±0.75% ID/g), which was not seen with labeled hMSCs. From 1 day to 10 days after injection, signals of bone uptake gradually accumulate, this bone-targeting phenomenon of ^{89}Zr was consistent with that reported previously [34]. Thus, the loss of ^{89}Zr in cells could be estimated by the radioactivity of the bones. Eggenhofer *et*

Fig. 11

The biodistribution of ^{89}Zr-oxine-labeled hMSCs and ^{89}Zr-oxalate at 10 days post-injection. ^{89}Zr-oxine-labeled hMSCs were mainly distributed in the liver ($7.35 \pm 1.41\%$ ID/g) and spleen ($8.48 \pm 1.20\%$ ID/g). ^{89}Zr-oxalate was mainly distributed in the bone ($4.77 \pm 0.35\%$ ID/g). **The difference was significant from that of the control at $P < 0.01$ level. All data were expressed as means ± SD.

al. demonstrated that some exogenous MSCs survived in the lungs within 24 hours of intravenous injection. After 24 hours, living MSCs disappeared from the lungs, but these lived MSCs did not reappear in the liver, spleen, kidneys, or bones, suggesting that they could not survive long-term in the recipient animals [31]. In this study, radioactivity signals were also found in the liver and spleen from 1 day to 10 days after injection, but we were unable to detect hMSCs in these organs by Q-PCR at 10 days post-injection (below the minimum quantitative limit), suggesting that Q-PCR analysis required a higher detection threshold compared to radiolabeling (e.g. a 10-fold increase in the number of hMSCs required for cardiac Q-PCR detection [35]). According to Eggenhofer *et al.*, even if the number of hMSCs reaches the threshold required for Q-PCR analysis, the radioactive signals in the liver and spleen might originate from hMSCs fragments or other endogenous cells that engulf hMSCs fragments, rather than live hMSCs. Because living hMSCs could not pass through the capillary bed of the lungs after intravenous injection. Immune cells may well be involved in this process. It had been hypothesized that apoptosis of infused cells could trigger an immunomodulatory response [36] and recently it was demonstrated that macrophages adapted an immunoregulatory function after phagocytosis of the dead hMSCs [37]. Further research must reveal which signals conduct this response through the body.

One potential limitation of direct cell labeling techniques is that cells inevitably lose a portion of the radiolabeled substance, resulting in in-vivo imaging results that cannot determine whether the signal is from the labeled cell or from an endogenous cell that engulfs the outflow signal, or from dead labeled cell debris, a common problem with all direct cell labeling techniques. To overcome this limitation, genetic labeling strategies may be more appropriate for long-term tracking of transplanted cells *in vivo*. This method requires genetic modification of donor cells *in vitro* to stably express a reporter protein that can selectively bind to the tracer [38]. Currently, although in-vivo imaging modalities have been largely used in studies of small animals, our ultimate goal is to apply this groundbreaking technology to the clinic to aid in understanding the distribution and fate of different stem cells in the human body. Large animals (pigs, dogs, monkeys, etc.) are most similar to humans in terms of body size, disease progression, body weight, and overall anatomy [39]. Therefore, a lot of researches are still needed on these animal models. In summary, we still have a lot of work to do in order to elucidate the mechanism and fate of hMSCs after transplantation and provide more reliable information for clinical applications.

Conclusion

This study showed that ^{89}Zr-oxine labeling preserved the functionality and characteristics of hMSCs, demonstrating the feasibility of this platform for tracking systemically delivered cells. This labeling method could be a valuable tool for the preclinical noninvasive assessment of various cell-based therapies. To further explore the potential of this approach, more work is needed to test this strategy in a variety of model systems and diseases treatments relevant to cell tracking and cell therapy.

Acknowledgements

Conflicts of interest

There are no conflicts of interest.

References

1 Fruhwirth GO, Kneilling M, de Vries IJM, Weigelin B, Srinivas M, Aarntzen EHJG. The potential of *In Vivo* imaging for optimization of molecular and cellular anti-cancer immunotherapies. *Mol Imaging Biol* 2018; **20**:696–704.

2 Volpe A, Kurtys E, Fruhwirth GO. Cousins at work: how combining medical with optical imaging enhances *in vivo* cell tracking. *Int J Biochem Cell Biol* 2018; **102**:40–50.

3 Cussó L, Mirones I, Peña-Zalbidea S, García-Vázquez V, García-Castro J, Desco M. Combination of single-photon emission computed tomography and magnetic resonance imaging to track 111in-oxine-labeled human mesenchymal stem cells in neuroblastoma-bearing mice. *Mol Imaging* 2014; **13**:10–20.

4 Gildehaus FJ, Haasters F, Drosse I, Wagner E, Zach C, Mutschler W, *et al.* Impact of indium-111 oxine labelling on viability of human mesenchymal stem cells *in vitro*, and 3D cell-tracking using SPECT/CT in vivo. *Mol Imaging Biol* 2011; **13**:1204–1214.

5 Gholamrezanezhad A, Mirpour S, Bagheri M, Mohamadnejad M, Alimoghaddam K, Abdolahzadeh L, *et al. In vivo* tracking of 111In-oxine labeled mesenchymal stem cells following infusion in patients with advanced cirrhosis. *Nucl Med Biol* 2011; **38**:961–967.

6 Charoenphun P, Meszaros LK, Chuamsaamarkkee K, Sharif-Paghaleh E, Ballinger JR, Ferris TJ, *et al.* [(89)Zr]oxinate4 for long-term *in vivo* cell tracking by positron emission tomography. *Eur J Nucl Med Mol Imaging* 2015; **42**:278–287.

7 Bansal A, Pandey MK, Demirhan YE, Nesbitt JJ, Crespo-Diaz RJ, Terzic A, *et al.* Novel (89)Zr cell labeling approach for PET-based cell trafficking studies. *EJNMMI Res* 2015; **5**:19.

8 Sato N, Wu H, Asiedu KO, Szajek LP, Griffiths GL, Choyke PL. (89) Zr-Oxine complex PET cell imaging in monitoring cell-based therapies. *Radiology* 2015; **275**:490–500.

9 Yang B, Brahmbhatt A, Nieves Torres E, Thielen B, McCall DL, Engel S, *et al.* Tracking and therapeutic value of human adipose tissue-derived mesenchymal stem cell transplantation in reducing venous neointimal hyperplasia associated with arteriovenous fistula. *Radiology* 2016; **279**:513–522.

10 Man F, Lim L, Volpe A, Gabizon A, Shmeeda H, Draper B, *et al.* In Vivo PET Tracking of (89)Zr-Labeled Vγ9Vδ2 T Cells to Mouse Xenograft Breast Tumors Activated with Liposomal Alendronate. *Mol Ther* 2019; **27**:219–229.

11 Asiedu KO, Koyasu S, Szajek LP, Choyke PL, Sato N. Bone marrow cell trafficking analyzed by (89)Zr-oxine positron emission tomography in a murine transplantation model. *Clin Cancer Res* 2017; **23**:2759–2768.

12 Patrick PS, Kolluri KK, Zaw Thin M, Edwards A, Sage EK, Sanderson T, *et al.* Lung delivery of MSCs expressing anti-cancer protein TRAIL visualised with 89Zr-oxine PET-CT. *Stem Cell Res Ther* 2020; **11**:256.

13 Rahmim A, Zaidi H. PET versus SPECT: strengths, limitations and challenges. *Nucl Med Commun* 2008; **29**:193–207.

14 Brenner W, Aicher A, Eckey T, Massoudi S, Zuhayra M, Koehl U, *et al.* 111In-labeled CD34+ hematopoietic progenitor cells in a rat myocardial infarction model. *J Nucl Med* 2004; **45**:512–518.

15 Gholamrezanezhad A, Mirpour S, Ardekani JM, Bagheri M, Alimoghadam K, Yarmand S, Malekzadeh R. Cytotoxicity of 111In-oxine on mesenchymal stem cells: a time-dependent adverse effect. *Nucl Med Commun* 2009; **30**:210–216.

16 Dominici M, Le Blanc K, Mueller I, Slaper-Cortenbach I, Marini F, Krause D, *et al.* Minimal criteria for defining multipotent mesenchymal stromal cells. The International Society for Cellular Therapy position statement. *Cytotherapy* 2006; **8**:315–317.

17 Pittenger MF, Mackay AM, Beck SC, Jaiswal RK, Douglas R, Mosca JD, *et al.* Multilineage potential of adult human mesenchymal stem cells. *Science* 1999; **284**:143–147.

18 Majumdar MK, Keane-Moore M, Buyaner D, Hardy WB, Moorman MA, McIntosh KR, Mosca JD. Characterization and functionality of cell surface molecules on human mesenchymal stem cells. *J Biomed Sci* 2003; **10**:228–241.

19 Devine SM, Peter S, Martin BJ, Barry F, McIntosh KR. Mesenchymal stem cells: stealth and suppression. *Cancer J* 2001; **7**(Suppl 2):S76–S82.

20 Raza K, Larsen T, Samaratunga N, Price AP, Meyer C, Matson A, *et al.* MSC therapy attenuates obliterative bronchiolitis after murine bone marrow transplant. *PLoS One* 2014; **9**:e109034.

21 Lopez-Santalla M, Hervas-Salcedo R, Fernandez-Garcia M, Bueren JA, Garin MI. Cell therapy with mesenchymal stem cells induces an innate immune memory response that attenuates experimental colitis in the long term. *J Crohns Colitis* 2020; **14**:1424–1435.

22 Liu L, Farhoodi HP, Han M, Liu G, Yu J, Nguyen L, *et al.* Preclinical evaluation of a single intravenous infusion of hUC-MSC (BX-U001) in rheumatoid arthritis. *Cell Transplant* 2020; **29**:963689720965896.

23 Ashraf S, Han IB, Park H, Lee SH. Role of RHEB in regulating differentiation fate of mesenchymal stem cells for cartilage and bone regeneration. *Int J Mol Sci* 2017; **18**:E880.

24 Sassoli C, Vallone L, Tani A, Chellini F, Nosi D, Zecchi-Orlandini S. Combined use of bone marrow-derived mesenchymal stromal cells (BM-MSCs) and platelet rich plasma (PRP) stimulates proliferation and differentiation of myoblasts *in vitro*: new therapeutic perspectives for skeletal muscle repair/regeneration. *Cell Tissue Res* 2018; **372**:549–570.

25 Zhou C, Wu XR, Liu HS, Liu XH, Liu GH, Zheng XB, *et al.* Immunomodulatory effect of urine-derived stem cells on inflammatory bowel diseases via downregulating Th1/Th17 immune responses in a PGE2-dependent manner. *J Crohns Colitis* 2020; **14**:654–668.

26 Lim JY, Im KI, Lee ES, Kim N, Nam YS, Jeon YW, Cho SG. Enhanced immunoregulation of mesenchymal stem cells by IL-10-producing type 1 regulatory T cells in collagen-induced arthritis. *Sci Rep* 2016; **6**:26851.

27 Lopez-Santalla M, Menta R, Mancheño-Corvo P, Lopez-Belmonte J, DelaRosa O, Bueren JA, *et al.* Adipose-derived mesenchymal stromal cells modulate experimental autoimmune arthritis by inducing an early regulatory innate cell signature. *Immun Inflamm Dis* 2016; **4**:213–224.

28 Abomaray FM, Al Jumah MA, Kalionis B, AlAskar AS, Al Harthy S, Jawdat D, *et al.* Human chorionic villous mesenchymal stem cells modify the functions of human dendritic cells, and induce an anti-inflammatory phenotype in CD1+ dendritic cells. *Stem Cell Rev Rep* 2015; **11**:423–441.

29 Chamberlain G, Fox J, Ashton B, Middleton J. Concise review: mesenchymal stem cells: their phenotype, differentiation capacity, immunological features, and potential for homing. *Stem Cells* 2007; **25**:2739–2749.

30 Jaiswal RK, Jaiswal N, Bruder SP, Mbalaviele G, Marshak DR, Pittenger MF. Adult human mesenchymal stem cell differentiation to the osteogenic or adipogenic lineage is regulated by mitogen-activated protein kinase. *J Biol Chem* 2000; **275**:9645–9652.

31 Eggenhofer E, Benseler V, Kroemer A, Popp FC, Geissler EK, Schlitt HJ, *et al.* Mesenchymal stem cells are short-lived and do not migrate beyond the lungs after intravenous infusion. *Front Immunol* 2012; **3**:297.

32 Scarfe L, Taylor A, Sharkey J, Harwood R, Barrow M, Comenge J, *et al.* Non-invasive imaging reveals conditions that impact distribution and persistence of cells after *in vivo* administration. *Stem Cell Res Ther* 2018; **9**:332.

33 Squillaro T, Peluso G, Galderisi U. Clinical trials with mesenchymal stem cells: an update. *Cell Transplant* 2016; **25**:829–848.

34 Abou DS, Ku T, Smith-Jones PM. *In vivo* biodistribution and accumulation of 89Zr in mice. *Nucl Med Biol* 2011; **38**:675–681.

35 Pittenger MF, Martin BJ. Mesenchymal stem cells and their potential as cardiac therapeutics. *Circ Res* 2004; **95**:9–20.

36 Thum T, Bauersachs J, Poole-Wilson PA, Volk HD, Anker SD. The dying stem cell hypothesis: immune modulation as a novel mechanism for progenitor cell therapy in cardiac muscle. *J Am Coll Cardiol* 2005; **46**:1799–1802.

37 Lu W, Fu C, Song L, Yao Y, Zhang X, Chen Z, *et al*. Exposure to supernatants of macrophages that phagocytized dead mesenchymal stem cells improves hypoxic cardiomyocytes survival. *Int J Cardiol* 2013; **165**:333–340.

38 Schug C, Gupta A, Urnauer S, Steiger K, Cheung PF, Neander C, *et al*. A Novel approach for image-guided (131)I therapy of pancreatic ductal adenocarcinoma using mesenchymal stem cell-mediated nis gene delivery. *Mol Cancer Res* 2019; **17**:310–320.

39 White FC, Roth DM, Bloor CM. The pig as a model for myocardial ischemia and exercise. *Lab Anim Sci* 1986; **36**:351–356.